# Reflectance measurement validation using acoustic horns

Daniel M. Rasetshwane[a] and Stephen T. Neely
*Boys Town National Research Hospital, Omaha, Nebraska 68131, USA*

(Received 11 November 2014; revised 27 August 2015; accepted 28 August 2015; published online 20 October 2015)

Variability in wideband acoustic reflectance (and absorbance) measurements adversely affects the clinical utility of reflectance for diagnosis of middle-ear disorders. A reflectance standard would encourage consistency across different measurement systems and help identify calibration related issues. Theoretical equations exist for the reflectance of finite-length exponential, conical, and parabolic acoustic horns. Reflectance measurements were repeatedly made in each of these three horn shapes and the results were compared to the corresponding theoretical reflectance. A method is described of adjusting acoustic impedance measurements to compensate for spreading of the wave front that propagates from the small diameter sound port of the probe to the larger diameter of the acoustic cavity. Agreement between measured and theoretical reflectance was less than 1 dB at most frequencies in the range from 0.2 to 10 kHz. Pearson correlation coefficients were greater than 0.95 between measured and theoretical *time-domain* reflectance within the flare region of the horns. The agreement suggests that the distributed reflectance of acoustic horns may be useful for validating reflectance measurements made in human ear canals; however, refinements to reflectance measurement methods may still be needed. © *2015 Acoustical Society of America*.
[http://dx.doi.org/10.1121/1.4930948]

[CAS] Pages: 2246–2255

## I. INTRODUCTION

Acoustic reflectance can noninvasively measure the response of the middle ear to sound stimulation in the ear canal. Reflectance has been observed to be sensitive to abnormal middle-ear states such as (1) positive and negative pressure in the middle-ear cavity, (2) a fluid-filled middle ear, (3) malleus or stapes fixation, (4) incudostapedial-joint disarticulation, (5) tympanic-membrane perforations, and (6) superior semicircular canal dehiscence. Because of its sensitivity to these pathological conditions, reflectance has been suggested for clinical diagnosis of various middle-ear disorders (e.g., Voss *et al.*, 2012; Nakajima *et al.*, 2012; Rosowski *et al.*, 2012; Merchant, 2014; Merchant *et al.*, 2015). However, reflectance measurements made with different measurement systems and made in different research laboratories can be variable. Methods to validate reflectance measurements are needed. We suggest using acoustic horns as a reflectance standard that would encourage consistency across different measurement systems and facilitate identification of problems with equipment, calibration, and data analysis.

Recently, Beranek and Mellow (2012) published theoretical equations for the transmission of pressure and volume velocity through finite-length acoustic horns with exponential, conical, and parabolic shapes. The calculation of reflectance at the horn input is straightforward from these equations. The aim of this study was to compare reflectance measurements made in exponential, conical, and parabolic horns to their corresponding theoretical reflectance, and assess whether these measurements may be useful for validating reflectance measured in the ear canal. This study extends our earlier theoretical study of infinite-length horns (Rasetshwane *et al.*, 2012) to the analysis of wave propagation in finite horns. As an initial step toward the creation of a reflectance standard, we focus on finite horn shapes for which exact solutions are known. We also focus on wave propagation through the flare region of the horns where reflection is spatially distributed.

Viscothermal effects and higher order modes of propagation result in propagation loses in actual physical horns. Keefe (1984) described procedures to account for these losses with regard to wave propagation in cylindrical ducts. We incorporate viscothermal propagation losses in our analysis of wave propagation in horns by approximating the continuously varying cross-sectional area of the horn with concatenated slices of thin cylindrical segments (e.g., Keefe, 1984; Milenkovic, 1987). The cylindrical-slice approach provides a very good approximation of wave propagation when both the number of tube sections and the sampling rate are high.

Normative databases for wideband acoustic immittance (WAI)—a grouping of ear-canal measurements that includes absorbance and reflectance (Rosowski *et al.*, 2013)—are currently being developed and considerable inter-subject and intra-subject variability has been reported among measurements. To demonstrate the variability in the measurements, Fig. 1 reproduces a total of five absorbance measurements from four studies (Rosowski *et al.*, 2012; Shahnaz *et al.*, 2013; Feeney *et al.*, 2014; and Groon *et al.*, 2015) made using four different measurement systems. Power reflectance is the squared magnitude of reflectance, and absorbance is the complement of power reflectance ($A = 1 - |R|^2$), so differences in absorbance are equal to differences in power

[a]Electronic mail: daniel.rasetshwane@boystown.org

 0001-4966/2015/138(4)/2246/10/$30.00 

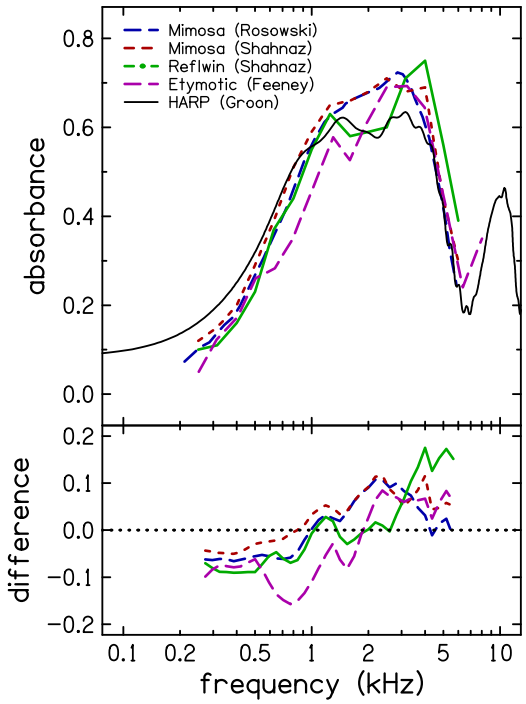


FIG. 1. (Color online) Variability in ear-canal absorbance measurements. The top panel shows a comparison of absorbance measurements made using the HARP, Mimosa, Reflwin Interacoustics and Etymōtic ER10C systems. The bottom panel shows differences in absorbance between the HARP measurements and the other measurements.

reflectance. Two sets of measurements (Rosowski *et al.*, 2012; Shahnaz *et al.*, 2013) were made with the Mimosa system (Mimosa Acoustics, Champaign, IL), one (Shahnaz *et al.*, 2013) with the Reflwin system (Interacoustics, Denmark), one (Feeney *et al.*, 2014) with the Etymōtic ER-10 C system (Etymōtic Research, Elk Grove Village, IL, USA), and one (Groon *et al.*, 2015) with the HARP system (Hearing Assessment Reformulation Project). The HARP system was developed by J. H. Siegel and S. Dhar for research studies at Northwestern University. All measurements were made in participants with normal hearing; however, cochlear hearing loss is not thought to have a significant effect on these measurements. Overall the measurements made with the different systems appear similar; they have similar low (between 0.5 and 1 kHz) and high (between 4 and 6 kHz) frequency slopes, and broad mid-frequency (between 1 and 4 kHz) peaks. However, the bottom panel, which plots the differences between the HARP measurements and the other measurements, shows that differences in absorbance between the measurements exist between 0.5 and 6 kHz. Across systems, differences in absorbance at a given frequency can be as large as 17%. Ideally, differences across systems should be small compared to typical intra-subject deviations across repeated measurements (e.g., Rosowski *et al.*, 2012, Fig. 5A; Voss *et al.*, 2013). Intra-subject variability is expect to decrease in coming years as measurement technology advances, thus increasing the need for consistency across measurement systems.

The variability in WAI measurements arises from factors related to study participants such as test ear (left vs right), sizes of the ear canal and middle-ear air space, gender, age, and ethnicity (e.g., Voss *et al.*, 2012; Shahnaz *et al.*, 2013; Abur *et al.*, 2014; Feeney *et al.*, 2014). Variability can also be caused by distortions from the measurement equipment and errors in Thévenin calibration, i.e., determination of Thévenin-equivalent parameters of the sound source (i.e., source impedance and pressure). Variability can arise from improper placement of the probe ear tip or from movement of the ear tip during data collection (e.g., Rosowski *et al.*, 2012; Abur *et al.*, 2014; Groon *et al.*, 2015). WAI variability has also been shown to depend on test frequency, with greater variability for middle to high frequencies compared to low frequencies (e.g., Werner *et al.*, 2010; Voss *et al.*, 2012). Different studies have reached different conclusions as to which of these factors contribute significantly to WAI variability. For example, Feeney *et al.*, (2014) reported a significant difference in WAI due to gender, while Shahnaz and Bork (2006) reported no significant difference. There is also test-retest variability in WAI measurements (e.g., Werner *et al.*, 2010; Vander Werff *et al.*, 2007).

Although the variability observed in normative data is smaller than the differences observed between these data and data from ears with middle-ear pathologies (e.g., Voss *et al.*, 2012; Nakajima *et al.*, 2012), the variability affects the diagnostic value of WAI, especially considering that the diagnosis of middle pathologies using absorbance, for example, is based on comparison of the shape of the absorbance functions in patient ears to a normative reference absorbance function. It is important to limit the contribution to this variability that is due to the measurement system. A reflectance validation procedure can facilitate this objective.

In Fig. 1, measurements made with the Mimosa systems extend only up to 6 kHz. Extending reflectance measurements to higher frequencies could improve the diagnostic value of reflectance and improve the resolution in the time-domain. The desirability of extending the frequency range of reflectance measurements above 6 kHz increases the need for validation because the assumption of plane wave propagation is questionable at higher frequencies. Spreading of the wave front from the small diameter sound port of the probe to the larger diameter of the acoustic cavity into which the probe is inserted creates an inertance in series with the acoustic impedance of the cavity. The added impedance of the spreading inertance increases in magnitude as frequency increases. The significance of the spreading impedance in various devices is presently unknown. However, its potential influence on reflectance measurements increases the need for validation standards. We provide a demonstration of the effect that this spreading impedance has on horn measurements, and also describe a method that can be used to minimize the effect.

A reflectance standard could serve as a means for validating measurements and for checking the consistency of measurement equipment. Measurements in acoustic horns with known reflectance may provide the basis for such validation. Comparison of measurement to theory can help examiners identify shifts in measurements that are due to

issues such as air leaks, errors in Thévenin calibration, movement of the probe and ear tip within the ear canal during measurements, and other intermittent equipment issues. Differences in probe placement can contribute to variability in measurements of WAI (e.g., Huang *et al.,* 2000; Rosowski *et al.,* 2012). Air leaks have the greatest effect at low frequencies where they cause absorbance to increase, admittance phase to decrease towards zero degrees and excessive noise in power reflectance (e.g., Rosowski *et al.,* 2012; Groon *et al.,* 2015). Air leaks can also lead to inaccuracies in the Thévenin calibration procedure (Keefe *et al.,* 2000). Errors in Thévenin calibration can lead to errors in calculations of the load impedance and increased WAI variability (e.g., Voss *et al.*, 2013). The ability to validate measurement would provide examiners with confidence in the reflectance measurements that they are collecting.

## II. METHODS

Recent advances in three-dimensional (3-D) printing have made it affordable and easier to acquire physical realizations of acoustic horns of various shapes. Horns with conical, parabolic, and exponential flares were 3-D printed using rigid nylon plastic material.[1] The horns were terminated with a flat cap at the mouth end in order to reduce external noise. The dimensions of the horns are provided in Fig. 2. For all three horn shapes, the horn flare, i.e., the region with increasing diameter between the throat and the mouth, has a length of 12 cm. The flare diameter is 1 cm at the throat, which we define as the reference point for axial distance, and expands to make the cross-sectional area $A(x) = 10\,\text{cm}^2$ at $x = 10$ cm. Cylindrical segments were added at each end of the flare region. The length of cylindrical segment at the throat is 2 cm to allow for insertion of the measurement probe. The length of the cylindrical segment at the mouth is 1 cm to facilitate placement of a terminating cap. Thus, the overall length of each horn was 15 cm. As can be observed in Fig. 2, the three horn shapes differ in their dependence of diameter function $D(x)$ on axial distance $x$. Therefore, the development of procedures to validate reflectance presented in this article focus on wave propagation over this region. The equations relating $D(x)$ to $x$ for the three horn shapes are presented in the Appendix.

### A. Equipment and measurements

Acoustic pressure measurements, from which impedance and reflectance measurements are obtained, were made using an extended-bandwidth research probe system (ER-10X, Etymōtic Research, Elk Grove Village, IL, USA). Each stimulus condition was repeated on each of the two sound sources of this system, providing two independent measurements. The measurement system was calibrated prior to data collection to determine the Thévenin-equivalent source impedance and pressure (Allen, 1986; Keefe *et al.,* 1992; Rasetshwane and Neely, 2011). Thévenin-equivalent source parameters are required for the transformation of acoustic pressure to acoustic impedance and reflectance. Stimulus delivery and data collection were monitored using locally developed software (EMAV; Neely and Liu, 1994). Artifact rejection based on the root-mean-square amplitude of the recordings of time-domain pressure was utilized. In this procedure, which is effective for rejecting transient artifacts, two consecutive sweeps were both discarded if they differed by a criterion amount.

A total of 12 artifact-free pressure measurements per sound source were made in each acoustic horn, with reseating of the probe after every fourth measurement. Measurements from the two sound sources were averaged to improve the signal-to-noise ratio. Probe reseating was done to simulate the variability arising from differences in probe insertion depth and ear tip compression.

A wideband linear-swept frequency chirp signal, generated digitally at a sampling rate of 48 kHz, with a frequency resolution of 5.86 Hz, was used as the stimulus. The stimulus level, determined using a sound level meter (System 824; Larson Davis, Provo, UT) with C weighting, was 60 dB sound pressure level. The duration of each stimulus/response buffer was 171 ms. All measurements were made in an acoustically shielded booth.

### B. Reflectance calculation

Our 3-D printed horns consist of three concatenated segments: (1) a 2-cm cylindrical segment at the throat, (2) a

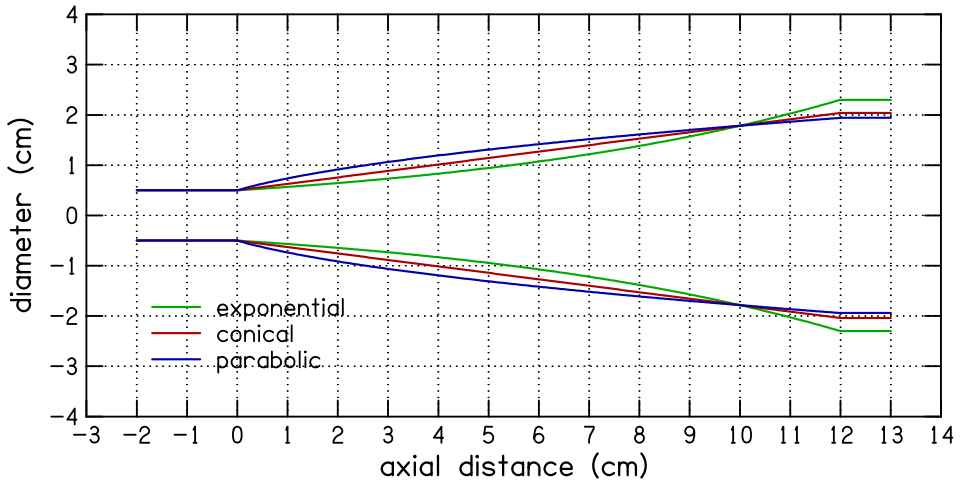


FIG. 2. (Color online) Horn diameter ($D$) as a function of axial distance ($x$) for exponential, conical, and parabolic horn shapes. The axial distance is in reference to the horn mouth.

flared segment with increasing diameter, and (3) a 1-cm cylindrical segment at the mouth. The flared segment had either the exponential, conical, or parabolic shape shown in Fig. 2. The acoustics of each segment of the horn can be represented by a two-port network that relates pressure and volume velocity at the left side to their counterparts at the right side. The transmission matrix that relates pressure and volume velocity at the left side of the first segment $[p_L(x, \omega), U_L(x, \omega)]$ to their counterparts at the right side of the third segment $[p_R(x, \omega), U_R(x, \omega)]$ is obtained by multiplication of the transmission matrices for each segment:

$$\begin{bmatrix} a_{11} & a_{12} \\ a_{21} & a_{22} \end{bmatrix} = \begin{bmatrix} a_{11}^1 & a_{12}^1 \\ a_{21}^1 & a_{22}^1 \end{bmatrix} \cdot \begin{bmatrix} a_{11}^2 & a_{12}^2 \\ a_{21}^2 & a_{22}^2 \end{bmatrix} \cdot \begin{bmatrix} a_{11}^3 & a_{12}^3 \\ a_{21}^3 & a_{22}^3 \end{bmatrix},$$
$$\begin{bmatrix} p_L \\ U_L \end{bmatrix} = \begin{bmatrix} a_{11} & a_{12} \\ a_{21} & a_{22} \end{bmatrix} \cdot \begin{bmatrix} p_R \\ U_R \end{bmatrix}. \quad (1)$$

The parameters of the transmission matrix $a_{11}$, $a_{12}$, $a_{21}$, and $a_{22}$, like the pressures $p_L$ and $p_R$, and volume velocities $U_L$ and $U_R$, are functions of both frequency $\omega$ and axial distance $x$, but a simplified notation will be used to avoid clutter. The superscripts denote segments 1–3. Using transmission matrices for the individual segments makes the matrix multiplication required to calculate the composite impedance easier. The acoustic impedance at the throat $Z_T$ is related to the acoustic radiation impedance at the mouth $Z_M$ through the transmission matrix parameters

$$Z_T = \frac{a_{11}Z_M + a_{12}}{a_{21}Z_M + a_{22}}. \quad (2)$$

The reflectance of the horn with impedance $Z$ is defined as

$$R = \frac{Z - Z_0}{Z + Z_0}, \quad (3)$$

where $Z_0(x) = \rho_0 c/S(x)$ is the characteristic impedance and depends on the cross-sectional area $S(x)$. $\rho_0$ and $c$ are the density of air and speed of sound in air, respectively. Alternately, $Z_0$ can be defined to be the surge component of horn impedance $Z$, i.e., the impulse at time zero when the impedance is transformed into the time domain. Combining Eqs. (2) and (3), the reflectance of the horn at the throat is

$$R_T = \frac{Z_M(a_{11} - a_{21}Z_0) + a_{12} - a_{22}Z_0}{Z_M(a_{11} + a_{21}Z_0) + a_{12} + a_{22}Z_0}. \quad (4)$$

Expressions for the transmission-matrix parameters of Eq. (1), i.e., $a_{11}$, $a_{12}$, $a_{21}$, and $a_{22}$, for a cylindrical tube and for parabolic, conical and exponential horn shapes are presented in the Appendix.

In order to include propagation losses due to viscothermal effects in our analysis, impedances for the flare region of the horns obtained using the above equations and equations presented in the Appendix were replaced by impedances calculated using the cylindrical-slice approximation method, as mentioned in Sec. I. In this method, the continuously varying cross-section area of the horn was replaced by a concatenation of a series of cylindrical slices. The composite impedance of the horn was then obtained by combining the impedances of the slices. Because methods for modeling viscothermal losses exist for cylindrical ducts, the cylindrical-slice approximation allows for modeling of these losses in horns. This method provides good estimation of wave propagation of the continuously varying cross section: Pearson correlations between the time-domain reflectance (TDR) obtained directly from the equations and the TDR obtained from the cylindrical-slice approximation without losses were equal to 1 for all three horn shapes. Observing agreement with the theoretical equations when the propagation loss was set to zero validates the cylindrical-slice approximation.

In actual measurements, the effective length of the cylindrical section at the throat was reduced by the insertion depth of the measurement probe. This effective length was estimated from acoustic pressure measurements. Based on this estimate, the effective length of the segment at the mouth was adjusted in the calculation of the theoretical reflectance. In measurements, the cap at the mouth of the horn manifests as an impedance composed of a resistance with an added stiffness. For calculations of theoretical reflectance, the resistance was estimated using an iterative procedure that minimizes the differences between values of the peak of the TDR for the measurements and theory. The stiffness was estimated from the imaginary part of the measured load admittance at low frequencies where the stiffness should dominate admittance (e.g., Groon *et al.*, 2015). The procedure for the stiffness estimation was to use a least-squares solution to the over-determined equation for calculating the coefficients of $[f\ 1/f]$ that best approximate the imaginary part of the load admittance at all frequencies in the range from 50 to 100 Hz. The cap impedance has minimal impact on time-domain comparisons between measurement and theory because such comparisons are restricted to the flare regions of the horn where the cap impedance has negligible effect.

Measured reflectance for the horns was calculated from the load impedance (after converting the acoustic pressure measurements to acoustic impedance using the Thévenin-equivalent impedance of the source) and the surge component of the load impedance $Z_0$ using Eq. (3). Our compensation for the spreading wave impedance was applied to the load impedance, prior to the calculation of reflectance. The compensation procedure modeled the contribution of the spreading wave to the load impedance by modeling the wavefront as a spreading diameter consisting of two adjacent conical segments. Parameters for the conical segment were determined by fitting this model to the measured impedance. The effect of the spreading wave was removed from the measured impedance by applying the inverse of the transmission matrix for the spreading segment to the measured load impedance. A transmission matrix for a cylindrical segment of the same length was then applied to measured impedance to restore the observed propagation delay.

Time-domain reflectance (TDR) was calculated as the inverse Fourier transform of the frequency-domain reflectance. Our measurements included noise for frequencies above 20 kHz, which limited our usable bandwidth. To mitigate the effect of the limited bandwidth and to reduce the

impact of measurement error, a Blackman window with a 20-kHz half-width was applied in the frequency-domain to reduce time-domain ringing (due to Gibbs phenomena) and to reduce contributions from higher frequencies where the measurements were less reliable. The resulting TDR was further smoothed by zero-padding the frequency-domain reflectance to 96 kHz, which is four times the measurement bandwidth. A Blackman window has less sideband leakage than equivalent length Hamming and Hann windows. This smoothing technique was previously used to process ear-canal reflectance data (Rasetshwane and Neely, 2011).

Pearson correlation between the measured and theoretical TDR was used as a metric for quantifying agreement between the measurements and theory. The correlation was calculated over a time interval that corresponds to the round trip travel through the flare region of the horns (0 to 0.58 ms). Calculating the correlations in the time-domain, as opposed to the frequency-domain, has the advantage that it excludes effects of the termination cap.

## III. RESULTS

Figure 3 shows frequency-domain reflectance for the three horn shapes using a logarithmic frequency axis. The solid lines show average reflectance, across the 12 repeated measurements. The error bars, included only at 1/3-octave intervals to avoid clutter, indicate $\pm 1$ standard deviation (SD). The top row shows reflectance magnitude and the bottom row shows group delay, defined as $\tau(\omega) = -\partial \angle R_T(\omega)/\partial\omega$ (i.e., minus the derivative of the phase of the reflectance) in ms. Measurements for different horn shapes are shown in separate columns as indicated at the top of the columns. The measurements have great variability below 0.2 kHz, as indicated by the large error bars. Above 0.2 kHz, variability in the measurements is small. Measurements from the three horns differ mainly in the size of their fine structure, i.e., peak-to-valley difference. The parabolic horn has the largest fine structure in both the reflectance magnitude (top panel) and the reflectance delay (bottom panel). The exponential horn has the smallest fine structure.

Figure 3 also shows theoretical reflectance for the three horn shapes (dashed lines). Overall the theoretical reflectances are similar to the measured reflectances—the nulls and peaks of both the theoretical reflectance magnitude and delay occur at the same locations as those of the measurements. The difference between measured and theoretical reflectance magnitude was less than 1 dB at most frequencies between 0.2 and 10 kHz. However, there are differences. The measured reflectance magnitude is larger than the theoretical reflectance magnitude at low frequencies, but smaller at high frequencies. That is, the measured reflectance decays with increase in frequency at a faster rate than the theoretical reflectance. The difference in magnitude is largest below 0.2 kHz and above 10 kHz, where the variability in the measured reflectance is largest. Last, for the parabolic horn, the sizes of the peak-to-null difference for the theoretical reflectance magnitude were larger than those of the measured reflectance.

The logarithmic-frequency axis of Fig. 3 provides a good visualization of the reflectance at low frequencies. To provide good visualization at high frequencies, Fig. 4 reproduces the reflectance of Fig. 3 but with a linear-frequency axis. The differences between measured and theoretical reflectance magnitude, described above, can be observed. The similarities in the reflectance delay between theory and measurements can also be observed. The differences among horns, the peak-to-null sizes, are also easier to see in this figure.

Time-domain reflectance was obtained as the inverse Fourier transform of the measured and theoretical reflectance of Figs. 3 and 4, as described in Sec. II. Figure 5 shows the

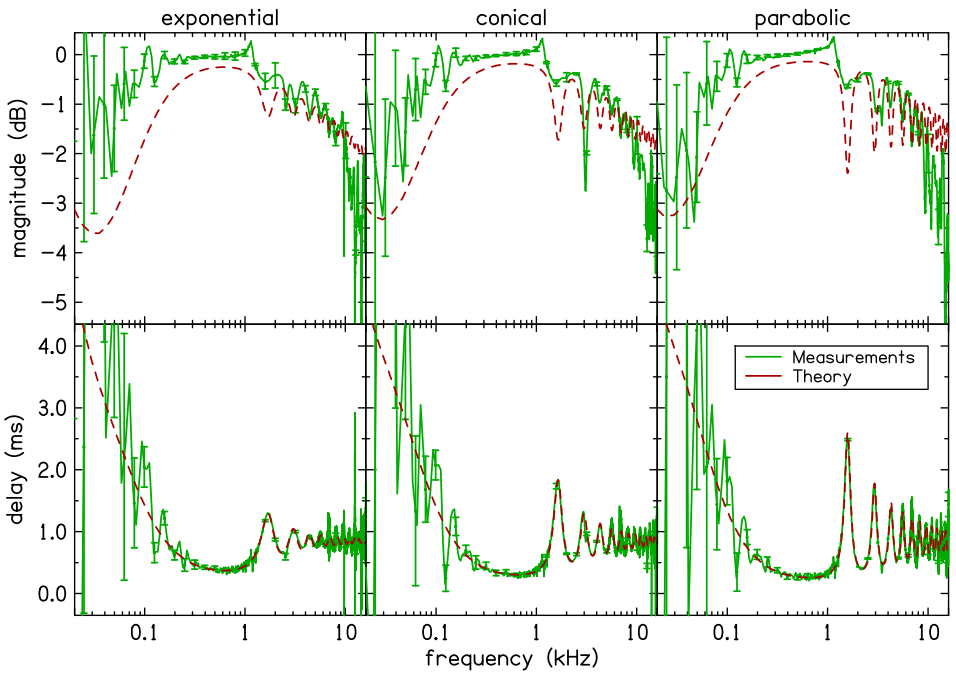


FIG. 3. (Color online) Average frequency-domain reflectance with *logarithmic* frequency axis for exponential (left column), conical (middle column), and parabolic horn (right column). The top row shows reflectance magnitude and the bottom row shows group delay. Measured reflectance is shown using solid lines and theoretical reflectance using dashed lines. The error bars represent $\pm 1$ SD.

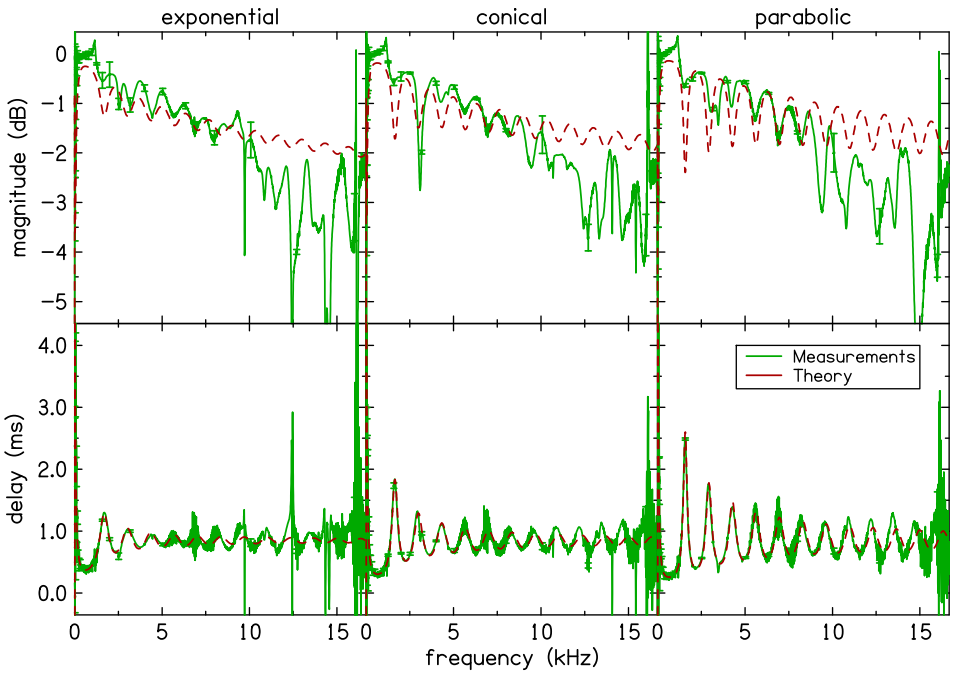


FIG. 4. (Color online) Average frequency-domain reflectance with *linear* frequency axis for exponential (left column), conical (middle column), and parabolic horn (right column). The top row shows reflectance magnitude and the bottom row shows group delay. Measured reflectance is shown using solid lines and theoretical reflectance using dashed lines. The error bars represent ±1 SD.

average TDR for measured (solid lines) and theoretical reflectance (dashed lines). The error bars, included only at 0.05 ms intervals, indicate ±1 SD. The large peak at 0.75 ms (which is clipped in the figure) is due to reflection from the cap at the mouth end of the horn. The impedance of the cap that was required for the theoretical quantities in order to match the measured TDR peak had average values of $129 + 14547/s$, $160 + 14715/s$, and $166 + 13681/s$ for the exponential, conical, and parabolic horns, respectively, where $s = j2\pi f$. The change in reflectance with time between time zero and the termination point depends on the horn shape. This demonstrates the distributed nature of the reflectance of acoustic horns, i.e., there is direct correspondence between the time-axis of the TDR and the axial distance from the throat of the acoustic horns (compare Fig. 5 to Fig. 2).

Pearson correlation between measured and theoretical TDR over the time-interval of 0 to 0.58 ms had a range of 0.95 to 0.98 for the exponential horn, with a mean of 0.97 and SD of 0.01. The range was 0.98 to 1.00 for the conical horn, with mean of 0.99 and SD of 0. And finally the range was 0.99 to 1.00 for the parabolic horn, with mean of 0.99 and SD of 0. All correlations were statistically significant with $p < 0.01$.

The TDR results shown in Fig. 5 include compensation to the measured load impedance for the spreading of the pressure wave at the plane of the probe. To demonstrate the effect of the spreading impedance, Fig. 6 shows measured TDR for the three horn shapes without compensation for the spreading impedance (solid lines). Theoretical TDR is shown using dashed lines. Recall that the wave front spreads as the sound wave propagates from the small diameter sound port of the measurement probe to the larger diameter of the acoustic horns. This spreading of the wave manifests approximately as a smoothed doublet centered at time zero (compare Fig. 6 to Fig. 5). The negative half of the doublet (at $t = 0.035$ ms in Fig. 6) apparently reduces the amplitude of

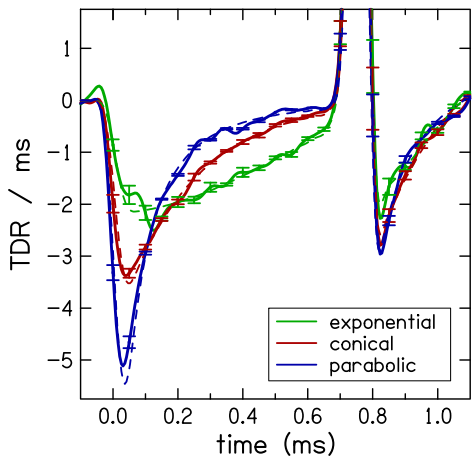


FIG. 5. (Color online) Time-domain reflectance of measurements and theory. Averages across the repeated measurements (solid lines) and theoretical reflectance (dashed lines) are superimposed, for comparison.

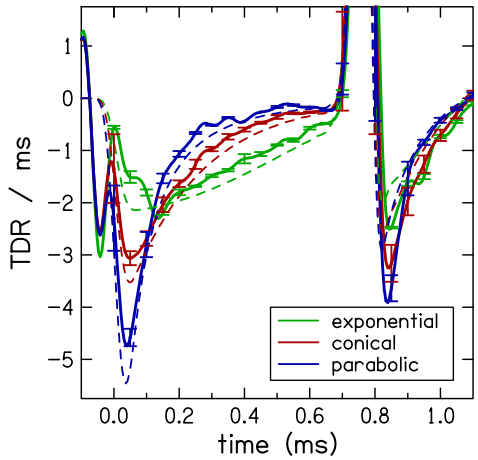


FIG. 6. (Color online) Demonstration of the effect of the wave spread inertance. Note that the large negative reflectance at $t = 0.035$ ms causes the negative reflectance in the range $0.1 < t < 0.8$ to be reduced.

the forward pressure beyond that location, as evidenced by reduced magnitude of the negative reflectance within the range $0.1 < t < 0.8$ of the uncompensated measured TDR in comparison to the theoretical TDR. Our compensation removes the doublet and improves the agreement with theoretical TDR.

## IV. DISCUSSION

Reflectance measurements made with different measurement systems and in different research laboratories can be variable. There is a need for methods to validate these measurements and facilitate identification of problems with equipment, calibration, and data analysis. Acoustic horns with known equations for the theoretical reflectance may provide the basis for this validation. As a first step toward the development of a reflectance standard, this study assessed whether measurements made in exponential, conical, and parabolic horns could be useful for validating reflectance.

In general, there was good agreement between measured and theoretical reflectance—the difference between measured and theoretical reflectance magnitude was less than 1 dB at most frequencies between 0.2 and 10 kHz. However, differences between measurements and theory were observed, especially in the low and high frequencies, where there was noise in the measurements. This noise is mainly due to distortion in the measurement equipment. The noise below 0.2 kHz may also have arisen due to the presence of air leaks, which have been shown to mostly affect reflectance measurements at low frequencies (Groon *et al.*, 2015). The smoothing applied to the TDR resulted in better agreement between measured and theoretical reflectance in the time-domain.

Theoretical reflectance magnitude is always less than 0 dB. The fact that the measured reflectance magnitude can be greater than 0 dB is an undesirable outcome and is presumably due to some limitation in the measurement method. Further development of the measurement method should attempt to reduce the deviation of the measured reflectance from the theoretical reflectance and eliminate any occurrence of reflectance magnitude greater than 0 dB.

The change in reflectance with time between time zero and the termination point depends on the horn shape. This demonstrates the distributed nature of the reflectance of acoustic horns, i.e., there is direct correspondence between the time-axis of the TDR and the axial distance from the throat of the acoustic horns. The distributed reflectance of acoustic horns suggests that ear-canal reflectance may also be distributed, i.e., the form of the time-domain reflectance, and the reflectance as a whole, depends on the curvature of the ear-canal. That is, the contribution of the ear canal to the measured reflectance (or absorbance) goes beyond a frequency-dependent delay, contrary to previous suggestions (e.g., Robinson *et al.*, 2013).

A large TDR peak, due to reflection at the cap at the mouth, was observed in the reflectance measurements. The height of the peak is directly proportional to the magnitude of the reflection occurring at the cap. For the measured reflectance, the height and width of this peak can potentially be reduced by matching the curvature of the cap to the geometry of the wave front. For the theoretical reflectance, use of an impedance function that accounts for the geometry of the wave front may, in theory, reduce the height and width of this peak. Inclusion of a mass term in this impedance may also result in a reflectance magnitude that decays with increase in frequency at a rate that is similar to that observed for the measurements. However, the height of this peak does not play a significant role in the conclusions of this article because our analysis focused on wave propagation through the flare region of the horns, where the equations in the Appendix are valid. Focusing on the flare region does not impose limitations on the ultimate applications of the present analysis—human ear-canal reflectance—since the length of the flare region used here (10 cm) is much greater than the length of a typical human ear canal (average of 2.6 cm according to Johansen, 1975).

Pearson correlation between measured and theoretical TDR were $\geq 0.95$. These correlations represent a very strong relationship between measured and theoretical reflectance over the flare region of the horns. The TDR correlations were based purely on the flare region of the horns (0 to 0.58 ms or 0 to 10 cm), and excluded effects of the termination cap. Improvements in the quality of the measurements, through the use of measurement systems with lower distortion and better Thévenin calibration techniques, can improve the correlations and even eliminate the need for windowing the frequency-domain reflectance prior to the calculation of the TDR. These improvements can further facilitate an additional metric for quantifying the agreement that is based on comparisons made in the frequency domain.

Our reflectance validation procedure was applied to horn measurements made with the HARP system (see Introduction) in order to evaluate whether our procedure can be extended to other measurement equipment. Pearson correlations for those measurements were similar to measurements obtained with ER-10X system. The correlations ranged from 0.99 to 1, with mean of 0.99 and SD of 0 for all three horn shapes. This demonstrates that the reflectance validation procedure is extensible to other measurement equipment, provided that they have bandwidth of up to 20 kHz.

The equations for wave propagation of Beranek and Mellow (2012) (see the Appendix) assume lossless plane-wave propagation. In actual physical horns, there are propagation losses due to viscothermal effects. In addition, wave propagation in actual horns is not one-dimensional; higher order modes of wave propagation are present at high frequency or when the diameter of the horn is no longer small compared to the wavelength of the propagating wave. Re-deriving the equation of Beranek and Mellow (2012) to account for viscothermal effects and higher order modes would be a daunting task, as evidenced by the fact that it has not yet been done, at least to the authors' knowledge. A more realistic approach is to use a cylindrical-slice approximation, as equations describing viscothermal losses in cylindrical ducts already exist. We used this approach to account

for viscothermal losses. The inclusion of viscothermal losses, which are marked by a reduction in the reflectance magnitude with increase in frequency, improved the agreement between measurements and theory at high frequencies.

We demonstrated that the spreading wave impedance could influence reflectance measurements. In the TDR, the contribution of the spreading wave to the load impedance approximates a smoothed doublet centered at time zero. In the frequency-domain, the effect of the spreading wave impedance is spread across frequency, and as a result more difficult to identify. The size of the spreading wave impedance depends on the difference between the diameters of the calibration and measurement cavities, with larger impedance for larger diameter differences. This impedance may thus contribute to variability in ear-canal reflectance measurements as there are differences across ears in the diameters at the entrance of the ear canal. In the current study, we applied a compensation for the spreading wave impedance to the load impedance. Compensation for wave spread appears to be important for accurate reflectance measurements.

The effect of the spreading wave impedance is similar to the Karal (1953) effect, in the sense that both arise from a step discontinuity. However, the two quantities are different. In our experience, a series inductance, which is equivalent to the Karal (1953) correction, was not sufficient to completely correct for the spreading-wave impedance. The spreading-wave impedance should not be confused with the Gibbs phenomenon, which is due to elimination of higher frequencies as a result of having a finite bandwidth. Wave spreading affects the load impedance even when all frequencies are present.

## V. CONCLUSION

Comparison of reflectance measurements in acoustic horns to corresponding theoretical reflectance can facilitate the establishment of consistency across different reflectance measurement systems and the identification of problems with these systems and with data analysis. Compensation for the spreading of the wave at the plane of the probe improves agreement of reflectance measurements with theoretical predictions. For the validation of reflectance measurements, we recommend Pearson correlations $\geq$0.95 in the TDR; however, further development of reflectance measurement methods could lead to better agreement with theoretical reflectance.


## ACKNOWLEDGMENTS

This research was supported by Grants Nos. R03 DC013982 (DMR), R01 DC8318 (STN), and P30 DC4662 from the National Institute of Health. We would like to thank Sara E. Fultz for her help with the reflectance measurements made with the HARP system and James D. Lewis for helpful suggestions on earlier versions of this manuscript.


## APPENDIX: RADIATION ADMITTANCE AND REFLECTANCE OF FINITE HORN

This section follows Beranek and Mellow (2012). Recall from Eq. (1) that a horn can be represented as a two-port network that relates pressure and volume velocity at the left side $[p_L(x, \omega), U_L(x, \omega)]$ to their counterparts at the right side $[p_R(x, \omega), U_R(x, \omega)]$:

$$\begin{bmatrix} p_L \\ U_L \end{bmatrix} = \begin{bmatrix} a_{11} & a_{12} \\ a_{21} & a_{22} \end{bmatrix} \cdot \begin{bmatrix} p_R \\ U_R \end{bmatrix}. \tag{A1}$$

To permit concatenation of adjacent sections by standard matrix multiplication, $U_R$ is defined coming out of the right side (mouth end), while $U_L$ is defined going into the left side (throat end). Because the transmission matrices described by Beranek and Mellow did not conform to this convention, their off-diagonal elements required application of a minus sign. The corrected matrix elements appear below.

### 1. Cylindrical tube

The equation expressing the diameter $D(x)$ of a cylindrical tube as a function of the axial distance $x$ is

$$D(x) = D_0, \tag{A2}$$

where $D_0$ is a constant, independent of axial distance $x$.

For a cylindrical tube, the matrix elements of Eq. (A1) are given by (Chipman, 1968)

$$a_{11} = \cosh(jkL), \tag{A3}$$

$$a_{12} = Z_0 \sinh(jkL), \tag{A4}$$

$$a_{21} = -\frac{1}{Z_0}\sinh(jkL), \tag{A5}$$

$$a_{22} = \cosh(jkL), \tag{A6}$$

where $k = \omega/c$ is the wave number and $c$ as the speed of sound in air.

### 2. Finite parabolic horn

The equation expressing the diameter $D(x)$ of the parabolic horn as a function of the axial distance $x$ is

$$D(x) = D_T\sqrt{1 + \alpha_p x}, \tag{A7}$$

where $\alpha_p$ is the flare constant and $D_T$ is the diameter of the throat. Values of the flare constant for the different horn shapes are given below.

For a finite parabolic horn, the matrix elements of Eq. (A1) are given by

$$a_{11} = -\frac{\pi}{2}kx_M(J_0(kx_T)Y_1(kx_M) - J_1(kx_M)Y_0(kx_T)), \tag{A8}$$

$$a_{12} = -j\frac{\rho_0 c}{S_M}\cdot\frac{\pi}{2}kx_M(J_0(kx_T)Y_0(kx_M) - J_0(kx_M)Y_0(kx_T)), \tag{A9}$$

$$a_{21} = -j\frac{S_T}{\rho_0 c}\cdot\frac{\pi}{2}kx_M(J_1(kx_T)Y_1(kx_M) - J_1(kx_M)Y_1(kx_T)), \tag{A10}$$

$$a_{22} = \frac{S_T}{S_M}\cdot\frac{\pi}{2}kx_M(J_1(kx_T)Y_0(kx_M) - J_0(kx_M)Y_1(kx_T)), \tag{A11}$$

where $S_T = \frac{1}{4}\pi D_T^2$ and $S_M = \frac{1}{4}\pi D_M^2 = \frac{1}{4}\pi D_T^2\ (1+\alpha_p L)$ are the cross-sectional areas of the throat and mouth, respectively, and $J_0$ and $J_1$ are the Bessel functions of the first kind and orders 1 and 2, respectively. $Y_0$ and $Y_1$ are the Bessel functions of the second kind and orders 1 and 2, respectively. $k = \omega/c$, $x_T$ and $x_M$ are related to axial location with $x_T = 1/\alpha_p$ and $x_M = (1/\alpha_p + L)$.

### 3. Finite conical horn

The equation expressing the diameter of the conical horn as a function of the axial distance is

$$D(x) = D_T(1+\alpha_c x). \tag{A12}$$

For a finite conical horn, the matrix elements of Eq. (A1) are given by

$$a_{11} = \sqrt{\frac{S_M}{S_T}}\left(\cos kL - \frac{1}{kx_M}\sin kL\right), \tag{A13}$$

$$a_{12} = -j\frac{\rho_0 c}{\sqrt{S_T S_M}}\sin kL, \tag{A14}$$

$$a_{21} = -j\frac{\sqrt{S_M S_T}}{\rho_0 c}\left\{\left(\frac{1}{kx_M} - \frac{1}{kx_T}\right)\cos kL + \left(1 + \frac{1}{k^2 x_M x_T}\right)\sin kL\right\}, \tag{A15}$$

$$a_{22} = \sqrt{\frac{S_T}{S_M}}\left(\cos kL + \frac{1}{kx_T}\sin kL\right), \tag{A16}$$

where $S_T = \frac{1}{4}\pi D_T^2$ and $S_M = \frac{1}{4}\pi D_T^2\ (1+\alpha_c L)$ are the cross-sectional areas of the throat and mouth, respectively. $k = \omega/c$, $x_T$, and $x_M$ are related to axial location with $x_T = 1/\alpha_c$ and $x_M = (1/\alpha_c + L)$.

### 4. Finite exponential horn

The equation expressing the diameter of the exponential horn as a function of the axial distance is

$$D(x) = D_T \exp(\alpha_e x). \tag{A17}$$

For a finite exponential horn, the matrix elements of Eq. (A1) are given by

$$a_{11} = \sqrt{\frac{S_M}{S_T}}(\cos(kL\cos\theta) - \tan\theta\sin(kL\cos\theta)), \tag{A18}$$

$$a_{12} = -j\frac{\rho_0 c}{\sqrt{S_T S_M}}\sec\theta\sin(kL\cos\theta), \tag{A19}$$

$$a_{21} = -j\frac{\sqrt{S_T S_M}}{\rho_0 c}\sec\theta\sin(kL\cos\theta), \tag{A20}$$

$$a_{22} = \sqrt{\frac{S_T}{S_M}}(\cos(kL\cos\theta) + \tan\theta\sin(kL\cos\theta)), \tag{A21}$$

where $S_T = \frac{1}{4}\pi D_T^2$ and $S_M = \frac{1}{4}\pi D_T^2\exp(2\alpha_e L)$ are the cross-sectional areas of the throat and mouth, respectively. $\theta = \arcsin(\alpha_e/k)$ and $k = \omega/c$.

In our 3D-printed examples, the flare parameters were selected such that each horn shape had the same diameter at $x = 0$ and $x = 10\,\text{cm}$: $\alpha_p = 1.173240$, $\alpha_c = 0.256825$, and $\alpha_e = 0.127207$.

[1]The horn designs are available online at https://www.shapeways.com/designer/neelys (Last visited 9/14/2015).


Abur, D., Horton, N. J., and Voss, S. E. (**2014**). "Intrasubject variability in power reflectance," J. Am. Acad. Audiol. **25**, 441–448.

Allen, J. B. (**1986**). "Measurement of eardrum acoustic impedance," in *Peripheral Auditory Mechanisms*, edited by J. B. Allen, J. L. Hall, A. Hubbard, S. T. Neely, and A. Tubis (Springer-Verlag, New York), pp. 44–51.

Beranek, L. L., and Mellow, T. J. (**2012**). *Acoustics: Sound Fields and Transducers* (Academic, Waltham, MA), pp. 407–438.

Chipman, R. A. (**1968**). *Theory and Problems of Transmission Lines* (McGraw-Hill, New York), pp. 126–155.

Feeney, M. P., Stover, B., Keefe, D. H., Garinis, A. C., Day, J. E., and Seixas, N. (**2014**). "Sources of variability in wideband energy reflectance measurements in adults," J. Am. Acad. Audiol. **25**, 449–461.

Groon, K. A., Rasetshwane, D. M., Kopun, J. G., Gorga, M. P., and Neely, S. T. (**2015**). "Effects of air-leaks on ear-canal acoustic absorbance," Ear Hear. **36**, 155–163.

Huang, G. T., Rosowski, J. J., Puria, S., and Peake, W. T. (**2000**). "A non-invasive method for estimating acoustic admittance at the tympanic membrane," J. Acoust. Soc. Am. **108**, 1128–1146.

Johansen, P. A. (**1975**). "Measurement of the human ear canal," Acustica **33**, 349–351.

Karal, F. C. (**1953**). "The analogous acoustical impedance for discontinuities and constrictions of circular cross section," J. Acoust. Soc. Am. **25**, 327–334.

Keefe, D. H. (**1984**). "Acoustical wave propagation in cylindrical ducts: Transmission line parameter approximations for isothermal and nonisothermal boundary conditions," J. Acoust. Soc. Am. **75**, 58–62.

Keefe, D. H., Folsom, R. C., Gorga, M. P., Vohr, B. R., Bulen, J. C., and Norton, S. J. (**2000**). "Identification of neonatal hearing impairment: Ear-canal measurements of acoustic admittance and reflectance in neonates," Ear Hear. **21**, 443–461.

Keefe, D. H., Ling, R., and Bulen, J. C. (**1992**). "Method to measure acoustic impedance and reflection coefficient," J. Acoust. Soc. Am. **91**, 470–485.

Merchant, G. R. (**2014**). "Functional measurements of ear pathology in patients and cadaveric preparations," Ph.D. dissertation, Massachusetts Institute of Technology, Cambridge, MA.

Merchant, G. R., Röösli, C., Niesten, M. E., Hamade, M. A., Lee, D. J., McKinnon, M. L., Ulku, C. H., Rosowski, J. J., Merchant, S. N., and Nakajima, H. H. (**2015**). "Power reflectance as a screening tool for the diagnosis of superior semicircular canal dehiscence," Otol. Neurotol. **36**, 172–177.

Milenkovic, P. (**1987**). "Acoustic tube reconstruction from noncausal excitation," IEEE Trans. Acoust. Speech Sign. Process. **35**, 1089–1100.

Nakajima, H. H., Pisano, D. V., Roosli, C., Hamade, M. A., Merchant, G. R., Mahfoud, L., Halpin, C. F., Rosowski, J. J., and Merchant, S. N. (**2012**). "Comparison of ear-canal reflectance and umbo velocity in patients with conductive hearing loss: A preliminary study," Ear Hear. **33**, 35–43.

Neely, S. T., and Liu, Z. (**1994**). "EMAV: Otoacoustic emission averager," Technical Memo No. 17 (Boys Town National Research Hospital, Omaha, NE).

Rasetshwane, D. M., and Neely, S. T. (**2011**). "Inverse solution of ear-canal area function from reflectance," J. Acoust. Soc. Am. **130**, 3873–3881.

Rasetshwane, D. M., Neely, S. T., Allen, J. B., and Shera, C. A. (**2012**). "Reflectance of acoustic horns and solution of the inverse problem," J. Acoust. Soc. Am. **131**, 1863–1873.
Robinson, S. R., Nguyen, C. T., and Allen, J. B. (**2013**). "Characterizing the ear canal acoustic impedance and reflectance by pole-zero fitting," Hear Res. **301**, 168–182.
Rosowski, J. J., Nakajima, H. H., Hamade, M. A., Mafoud, L. M., Merchant, G. R., Halpin, C. F., and Merchant, S. N. (**2012**). "Ear-canal reflectance, umbo velocity, and tympanometry in normal-hearing adults," Ear Hear. **33**, 19–34.
Rosowski, J. J., Stenfelt, S., and Lilly, D. (**2013**). "An overview of wideband immittance measurements techniques and terminology: You say absorbance, I say reflectance," Ear Hear. **34**, 9S–16S.
Shahnaz, N., and Bork, K. (**2006**). "Wideband reflectance norms for Caucasian and Chinese young adults," Ear Hear. **27**, 774–788.
Shahnaz, N., Feeney, M. P., and Schairer, K. S. (**2013**). "Wideband acoustic immittance normative data: Ethnicity, gender, aging, and instrumentation," Ear Hear. **34**, 27S–35S.
Vander Werff, K. R., Prieve, B. A., and Georgantas, L. M. (**2007**). "Test-retest reliability of wideband reflectance measures in infants under screening and diagnostic test conditions," Ear Hear. **28**, 669–681.
Voss, S. E., Merchant, G. A., and Horton, N. J. (**2012**). "Effects of middle-ear disorders on power reflectance measured in cadaveric ear canals," Ear Hear. **33**, 195–208.
Voss, S. E., Stenfelt, S., Neely, S. T., and Rosowski, J. J. (**2013**). "Factors that introduce intrasubject variability into ear-canal absorbance measurements," Ear Hear. **34**, 60S–64S.
Werner, L. A., Levi, E. C., and Keefe, D. H. (**2010**). "Ear-canal wideband acoustic transfer functions of adults and two-to nine-month-old infants," Ear Hear. **31**, 587–598.